Proc. Estonian Acad. Sci. Phys. Math., 2006, **55**, 2, 112–127

On real and imaginary algorithms of optical tensor field tomography

Hillar Aben, Andrei Errapart, and Leo Ainola

Institute of Cybernetics at Tallinn University of Technology, Akadeemia tee 21, 12618 Tallinn, Estonia; aben@ioc.ee

Received 25 January 2006

Abstract. In optical tensor field tomography either the dielectric tensor or the stress tensor has to be determined. In experiments either interferometric measurement of the absolute optical retardations or comparatively simple measurement of the relative optical retardations can be used. The paper analyses main differences of tomographic algorithms for the dielectric and stress tensor fields for both methods of optical measurements. It also shows that a recently published algorithm for tomographic measurement of the dielectric tensor field is wrong in principle.

Key words: photoelasticity, tomography, dielectric tensor, stress tensor, 3D stress analysis.

1. INTRODUCTION

Tomography is a powerful method for the analysis of the internal structure of different objects, from human bodies to parts of atomic reactors [1–3]. In tomography a certain radiation (X-rays, protons, acoustic waves, light, etc.) is passed through a section of the object in many directions, and properties of the radiation after it has passed the object (intensity, phase, deflection, etc.) are measured on many rays. Experimental data $g(l,\theta)$ for different values of the angle θ (Fig. 1) are called projections.

If $f(r,\varphi)$ is the function, which determines the distribution of a certain parameter of the field, experimental data for a real pair l,θ can be expressed by the Radon transform of the field

$$g(l,\theta)=\int_{-\infty}^{\infty} f(r,\varphi)\mathrm{d}z. \tag{1.1}$$

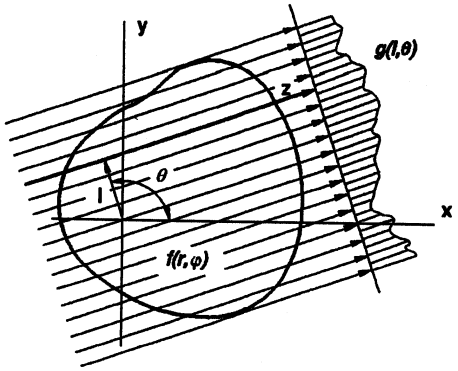

Fig. 1. Schema of tomographic measurements.

When projections for many values of θ have been recorded, the function $f(r,\varphi)$ is determined from the Radon inversion:

$$f(r,\varphi)=\frac{1}{2\pi^2}\int_0^{\pi}\mathrm{d}\theta\int_{-E}^{E}\frac{\partial g(l,\theta)}{\partial l}\frac{\mathrm{d}l}{r\cos(\theta-\varphi)-l}. \tag{1.2}$$

Many numerical algorithms for solving Eq. (1.2) have been elaborated [1,2].

The question arises whether it is possible to determine tomographically also tensor fields in 3D objects. This problem is not trivial for the following reason. Classical tomography considers only determination of scalar fields, i.e., every point of the field is characterized by a single number (the coefficient of attenuation of the X-rays, acoustic or optical index of refraction, etc.). Since stress is a tensor, in stress field tomography every point of the field is characterized by six numbers. Thus the problem is much more complicated in principle, since Radon inversion for the tensor field does not exist. Let us mention that while about one hundred books are devoted to scalar field tomography, only one book, written by Sharafutdinov [4], deals with mathematical problems of tensor field tomography.

In science and engineering it is often necessary to determine tensor fields in 3D objects. For example, measurement of the dielectric tensor field is important in investigating plasma jets [5] and measuring the Kerr effect caused by an electric field [6,7]. Stresses in 3D transparent objects are characterized by a stress tensor field. Determination of the stress tensor field is important for designing constructions using photoelasticity and for measuring residual stress in glass [8,9].

In the case of a scalar field the influence of a point of the field on the passing radiation does not depend on the direction of the radiation, since geometrically a scalar is represented by a sphere. For example, the extinction coefficient of the X-rays does not depend on the direction in which the X-rays pass the material.

A tensor is geometrically described by an ellipsoid with three different principal components $(\varepsilon_1,\varepsilon_2,\varepsilon_3)$ and their directions (Fig. 2). In optical tensor

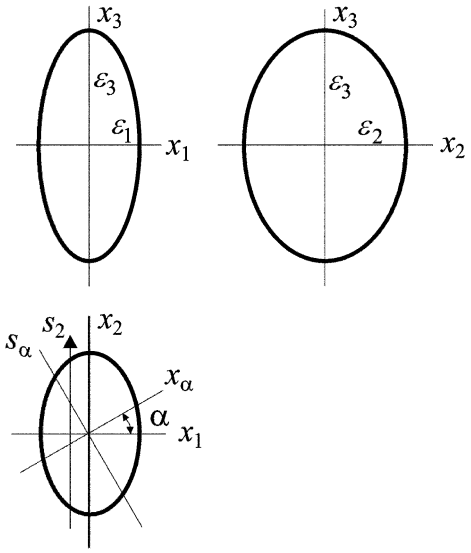

Fig. 2. Dielectric ellipsoid.

field tomography usually polarized radiation is used. Polarization of the radiation is influenced by the components of the dielectric tensor, which are located in the plane perpendicular to the direction of the radiation. For example, for radiation direction x_1 polarization is influenced by the components ε_2 and ε_3 of the dielectric tensor, for radiation direction x_2 by the components ε_1 and ε_3, etc. If the radiation passes through the section x_1x_2 obliquely along the direction s_α, polarization is influenced (Fig. 2) by the components ε_3 and

$$\varepsilon_\alpha = \varepsilon_1 \cos^2 \alpha + \varepsilon_2 \sin^2 \alpha . \tag{1.3}$$

The section of the dielectric ellipsoid that is formed by the plane perpendicular to an arbitrary ray z (Fig. 3) is an ellipse. This ellipse can be optically characterized by the components ε_{11}, ε_{22}, and ε_{12} of the dielectric tensor. The axes of the ellipse are called quasiprincipal axes and they form an angle φ with the x axis. Quasiprincipal values of the dielectric tensor in the xy plane, ε'_{11} and ε'_{22}, together with the angle φ, determine also the influence of the point of the tensor field on the passing radiation in the direction of $x_3 = z$ (Fig. 3).

One of the key problems in tensor field tomography is caused by the fact that in the general case the quasiprincipal directions of birefringence are not constant but rotate on the light ray. That is, φ is a function of z. Thus the question arises as to what can be measured in optical tensor field tomography and how the measurement data are related to the parameters of the tensor field. To elucidate this problem, we have to recall some principal postulates of the optics of twisted anisotropic optical media [10–12].

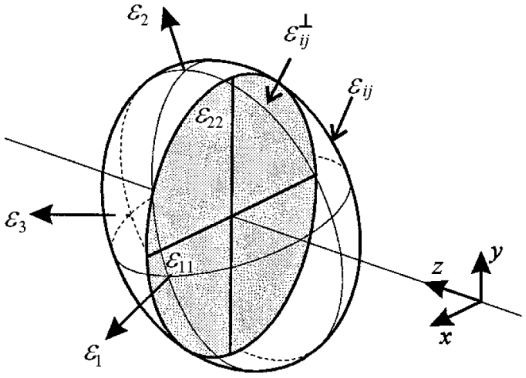

Fig. 3. The polarization of light is influenced by the components of the dielectric tensor which lie in the xy plane, perpendicular to the wave normal z.

2. INTEGRATED PHOTOELASTICITY

2.1. The general case

In integrated photoelasticity [11] a transparent 3D specimen is placed in an immersion tank, and a beam of polarized light is passed through the specimen. The transformation of the polarization of the light is measured on many light rays and for many azimuths of the light beam. The measurement data are related to the stress field in a complicated way.

The propagation of polarized light in the direction of the z axis through a 3D inhomogeneous birefringent medium is governed by the following equations [11]:

$$\frac{\mathrm{d}E_1}{\mathrm{d}z} = -i\frac{1}{2}C(\sigma_{11}-\sigma_{22})E_1 - iC\tau_{12}E_2, \tag{2.1}$$

$$\frac{\mathrm{d}E_2}{\mathrm{d}z} = -iC\tau_{12}E_1 + i\frac{1}{2}C(\sigma_{11}-\sigma_{22})E_2, \tag{2.2}$$

where E_1 and E_2 denote components of the electric vector along the x_1 and x_2 axes, C is the photoelastic constant, and σ_{11}, σ_{22}, and τ_{12} are components of the stress tensor in the x_1x_2 plane. The solution of Eqs (2.1) and (2.2) can be expressed as [11]

$$\begin{pmatrix} E_{1_*} \\ E_{2_*} \end{pmatrix} = U \begin{pmatrix} E_{10} \\ E_{20} \end{pmatrix}, \tag{2.3}$$

where E_{10}, E_{20} are the components of the incident light vector and E_{1_*}, E_{2_*} describe polarization of the light that emerges from the specimen. The matrix U

is a two-by-two unitary unimodular matrix, which in the general case can be written as

$$U = \begin{pmatrix} e^{i\xi}\cos\theta & e^{i\zeta}\sin\theta \\ -e^{-i\zeta}\sin\theta & e^{-i\xi}\cos\theta \end{pmatrix}, \tag{2.4}$$

where ξ, ζ, and θ are functions of the stress distribution between the points of entrance and emergence of the light.

Analysis of the transformation matrix (2.4) has shown that there always exist two perpendicular directions of the polarizer at which the light emerging from the medium is linearly polarized. The directions of polarization of the incident and emerging light are called the primary and secondary characteristic directions [10,11] and are determined through the angles α_0 and α_* as follows:

$$\tan 2\alpha_0 = \frac{\sin(\zeta+\xi)\sin 2\theta}{\sin 2\xi\cos^2\theta - \sin 2\zeta\sin^2\theta}, \tag{2.5}$$

$$\tan 2\alpha_* = \frac{\sin(\zeta-\xi)\sin 2\theta}{\sin 2\xi\cos^2\theta + \sin 2\zeta\sin^2\theta}. \tag{2.6}$$

Due to their exceptional physical properties, the characteristic directions can be measured experimentally [11,13,14]. It is also possible to measure the characteristic optical retardation Δ_* between the secondary characteristic vibrations:

$$\cos\Delta_* = \cos 2\xi\cos^2\theta + \cos 2\zeta\sin^2\theta. \tag{2.7}$$

If the characteristic parameters α_0, α_*, and Δ_* are determined experimentally on a light ray, it is possible to calculate the parameters ξ, ζ, and θ of the transformation matrix U:

$$\tan\xi = \frac{\cos(\alpha_0+\alpha_*)}{\cos(\alpha_0-\alpha_*)}\tan\frac{\Delta_*}{2}, \tag{2.8}$$

$$\tan\zeta = \frac{\sin(\alpha_0+\alpha_*)}{\sin(\alpha_0-\alpha_*)}\tan\frac{\Delta_*}{2}, \tag{2.9}$$

$$\tan\theta = \frac{\cos\xi}{\cos\zeta}\tan(\alpha_0-\alpha_*) = \frac{\sin\xi}{\sin\zeta}\tan(\alpha_0+\alpha_*). \tag{2.10}$$

Since the parameters ξ, ζ, and θ are determined in a nonlinear way by the stress distribution on the ray, in the general case the inverse problem of integrated photoelasticity is very complicated.

The parameters ξ, ζ, and θ of the transformation matrix can be calculated from the experimentally measured characteristic parameters α_0, α_*, and Δ_* using Eqs (2.8)–(2.10). The circumstance that ξ, ζ, and θ depend on the stress

distribution along the light ray opens, at least in principle, a possibility of determining the 3D stress field tomographically. Such an algorithm may be called *nonlinear tensor field tomography*, because the basic equations (2.8)–(2.10) are nonlinear. This is a principal difference from classical tomography, which may be called *linear tomography*, since it is based on line integrals (1.1) of the field.

With Eqs (2.1) and (2.2) we have formulated the problem of light propagation in the stress tensor field. If the reason for optical birefringence is not known, the problem can be formulated for the dielectric tensor field. In this case Eqs (2.1) and (2.2) are written as [11]

$$\frac{\mathrm{d}E_1}{\mathrm{d}z} = -i\frac{1}{2}C'(\varepsilon_{11} - \varepsilon_{22})E_1 - iC'\varepsilon_{12}E_2, \tag{2.11}$$

$$\frac{\mathrm{d}E_2}{\mathrm{d}z} = -iC'\varepsilon_{12}E_1 + i\frac{1}{2}C'(\varepsilon_{11} - \varepsilon_{22})E_2. \tag{2.12}$$

Let us mention that the matrix U in Eq. (2.3) is unitary and unimodular only if in the coefficients of Eqs (2.1) and (2.2) or (2.11) and (2.12) there appear only differences of the normal components of the stress tensor $(\sigma_{11} - \sigma_{22})$ or of the dielectric tensor $(\varepsilon_{11} - \varepsilon_{22})$.

Nonlinear photoelastic tomography has been considered by several authors [15–19]. In these papers the tomographic method is mostly described only verbally. Neither numerical nor physical experiments have been carried out to test the validity of the suggested algorithms. Thus, elaboration of photoelastic tomography on the basis of nonlinear relationships of integrated photoelasticity has not been successful up to now.

2.2. Linear approximation

Equations (2.1) and (2.2) can be written in the matrix form as

$$\frac{\mathrm{d}E}{\mathrm{d}z} = AE. \tag{2.13}$$

Expanding the solution of Eq. (2.13) into Neumann series [20], we obtain

$$U = I + \int_{z_0}^{z} A(\mathrm{z}_1)\mathrm{d}z_1 + \int_{z_0}^{z} \mathrm{d}z_1 A(z_1) \int_{z_0}^{z_1} \mathrm{d}z_2 A(z_2) + \ldots \tag{2.14}$$

In linear approximation we have

$$U = I + \int_{z_0}^{z} A(\mathrm{z})\,\mathrm{d}z. \tag{2.15}$$

It follows that in linear approximation an inhomogeneous birefringent medium can be considered as a birefringent plate ($\alpha_0 = \alpha_* = \alpha$). It is possible to measure the parameter of the isoclinic α and the integrated relative optical retardation Δ_*, which are expressed through the integrals of the components of the stress tensor [20]:

$$\Delta_* \cos 2\alpha = C \int_{z_0}^{z} (\sigma_{11} - \sigma_{22}) \mathrm{d}z, \tag{2.16}$$

$$\Delta_* \sin 2\alpha = 2C \int_{z_0}^{z} \tau_{12} \mathrm{d}z. \tag{2.17}$$

3. TWO OPTICAL MEASUREMENT METHODS

In passing polarized light through optically anisotropic objects two measurement methods can be applied [8]: (1) measurement of absolute optical retardations with an interferometer or (2) measurement of relative optical retardations between light vibrations along principal birefringence axes with a polariscope. To explain the principal difference between these methods, let us consider a most simple case, a dielectric medium with constant principal axes (Fig. 2).

By interferometric measurements, if polarized light is passed through the medium in the direction x_3 and the plane of light vibrations is parallel to x_1, absolute optical retardation Δ_1^{abs} can be measured:

$$\Delta_1^{\mathrm{abs}} = C'' \int \varepsilon_1 \mathrm{d}x_3, \tag{3.1}$$

where C'' is a constant that depends on the wavelength.

If the plane of vibration is parallel to x_2, we have

$$\Delta_2^{\mathrm{abs}} = C'' \int \varepsilon_2 \mathrm{d}x_3. \tag{3.2}$$

Passing light through the medium in the direction of x_1 with the plane of vibration x_3, we obtain

$$\Delta_3^{\mathrm{abs}} = C'' \int \varepsilon_3 \mathrm{d}x_1. \tag{3.3}$$

Thus, integrals of the components of the dielectric tensor can be obtained by interferometric measurements. These data may be used as a basis for tomographic algorithms. If the birefringence is caused by the photoelastic effect, in Eqs (3.1)–(3.3) we have to replace ε_j by components of the stress tensor σ_j. Absolute optical retardations can be measured with interferometers.

Photoelastic measurements are carried out mostly with polariscopes, which usually contain polaroids and quarter-wave plates [8,13,14]. Polariscopes permit

measuring the parameters of the polarization ellipse. These parameters depend only on the ratio of vibration amplitudes along the principal birefringence axes and on the relative optical retardation between these vibrations. The theory of integrated photoelasticity has been developed assuming that only relative optical retardations are measured [10,11].

Using standard polariscopes, in the same dielectric medium (Fig. 2) the following integrals can be measured:

$$\Delta_{12} = C'' \int (\varepsilon_1 - \varepsilon_2)\,\mathrm{d}x_3,\ \Delta_{23} = C'' \int (\varepsilon_2 - \varepsilon_3)\,\mathrm{d}x_1,\ \Delta_{31} = C'' \int (\varepsilon_3 - \varepsilon_1)\,\mathrm{d}x_2, \qquad (3.4)$$

or

$$\Delta_{12} = C' \int (\sigma_1 - \sigma_2)\,\mathrm{d}x_3,\ \Delta_{23} = C' \int (\sigma_2 - \sigma_3)\,\mathrm{d}x_1,\ \Delta_{31} = C' \int (\sigma_3 - \sigma_1)\,\mathrm{d}x_2. \qquad (3.5)$$

If light passes the medium in the direction of s_α, we have

$$\Delta_\alpha = C'' \int (\varepsilon_3 - \varepsilon_\alpha)\,\mathrm{d}s_\alpha. \qquad (3.6)$$

Thus no information about single components of the dielectric tensor can be obtained.

When developing the theory of characteristic directions on the basis of Eqs (2.1) and (2.2) it was assumed that experimentally only relative optical retardations are measured. Therefore, with suitable transformations the absolute phases of the components of the light vectors E_1 and E_2 were eliminated from the equations. Polarization of light is completely determined by the relative optical retardation and by the amplitude ratio of E_1 and E_2.

4. TOMOGRAHPY OF THE DIELECTIRC TENSOR FIELD

4.1. Measuring absolute optical retardations

Schupp [21,22] has developed a method for the tomography of the dielectric tensor field using interferometric measurement of absolute optical retardations. Such measurements are carried out by rotating the test object around a number of axes. In linear approximation integrals (3.1)–(3.3) permit determination of the distribution of the normal components of the stress tensor by rotating the test object around the x_1, x_2, and x_3 axes. Additional tomographic measurements permit determination of other dielectric tensor components as well. Equations (3.1) and (3.2) can be generalized for the case when the orientation of the dielectric tensor axes is arbitrary.

The method developed in [21,22] is mathematically correct and its applicability has been proved with numerical and physical experiments. Unfortunately, the author had to confess that he was able to obtain only qualitative results concerning the dielectric tensor field in his test object. That is due to the unavoidable

measurement errors when by interferometric measurements the test object is placed in an immersion tank.

4.2. Measuring relative optical retardations

Experimentally it is much simpler to measure in photoelastic tomography the characteristic parameters: the characteristic angles α_0 and α_* and the relative characteristic optical retardation Δ_*. However, in the general case the problem is highly complicated. It has been considered by Kubo and Nagata [15,23]. Due to evident complications with solving the problem, Kubo has discussed also application of the scattered light method [24].

A comparatively simple case is measurement of the Kerr effect if the direction of the electric field is constant. In the case of the Kerr effect the dielectric tensor is an ellipsoid of rotation. Thus, $\varepsilon_1 - \varepsilon_2$ characterizes the Kerr effect and the dielectric tensor field can be determined using methods of scalar field tomography [6].

The particular case of axisymmetric dielectric tensor fields has been considered in [25]. Some practical results have been obtained in the case of the axisymmetric Kerr effect [7].

Hammer and Lionheart [26] describe an algorithm for tomographic measurement of the dielectric tensor field. Instead of the system of equations (2.11) and (2.12) they use the equations

$$\frac{\mathrm{d}E_1}{\mathrm{d}z} = -i\frac{1}{2}C''(\varepsilon_{11} - \varepsilon_0)E_1 - iC''\varepsilon_{12}E_2, \tag{4.1}$$

$$\frac{\mathrm{d}E_2}{\mathrm{d}z} = -iC''\varepsilon_{12}E_1 - i\frac{1}{2}C''(\varepsilon_{22} - \varepsilon_0)E_2, \tag{4.2}$$

where $\varepsilon_0 = (\varepsilon_{11} + \varepsilon_{22} + \varepsilon_{33})/3$.

This presentation of the equations of integrated photoelasticity presumes that absolute optical retardations are measured. However, in [26] it is assumed that the characteristic parameters are measured experimentally. Unfortunately, with the system of equations (4.1) and (4.2), the matrix U (Eq. (2.3)) is not unimodular and the theory of characteristic directions is not valid.

The authors of [26] express the matrix U in the form

$$U = S(\Delta_*, \alpha_0, \alpha_*)\exp(i\Phi), \tag{4.3}$$

where Φ is the global phase of the transfer matrix U. Contrary to the claims of the authors, it is impossible to determine Φ without interferometric measurements.

Finally, relationship (2.16) is obtained in [26], which with the notations of the present paper can be written as

$$\frac{\Delta_*}{2}\cos 2\alpha = C\frac{\pi}{\lambda}\int_{z_0}^{z}(\varepsilon_{22}-\varepsilon_0)\mathrm{d}z. \tag{4.4}$$

Here $\alpha = \alpha_0 = \alpha_*$, since in the case of linear approximation the birefringent medium is equivalent to a birefringent plate with an azimuth of the principal directions equal to α. The right side of Eq. (4.4) can be measured only with interferometric methods. Thus Eq. (4.4) does not give the value of $\varepsilon_{22}-\varepsilon_0$ and the tomographic algorihm [26] is wrong in principle. However, in the case of weak birefringence we have

$$\varepsilon_0 = \frac{1}{2}(\varepsilon_{11}+\varepsilon_{22}), \tag{4.5}$$

where ε_{11} and ε_{22} are the quasiprincipal values of the dielectric tensor in the plane x_1x_2.

Introducing Eq. (4.5) into (4.4), we obtain

$$\frac{\Delta_*}{2}\cos 2\alpha = C\frac{\pi}{2\lambda}\int_{z_0}^{z}(\varepsilon_{11}-\varepsilon_{22})\mathrm{d}z. \tag{4.6}$$

Equation (4.6) confirms that if only relative characteristic optical retardations are measured, information can be obtained only about the integrals of $\varepsilon_{11}-\varepsilon_{22}$, $\varepsilon_{22}-\varepsilon_{33}$, $\varepsilon_{33}-\varepsilon_{11}$, and ε_{12}, ε_{23}, and ε_{31}. No information about the normal components of the dielectric tensor can be obtained separately. Equation (4.6) does not give much hope to build a tomographic algorithm for the analysis of a dielectric tensor field in the general case.

5. TOMOGRAPHY OF THE STRESS FIELD

It is well known that *a priori* information may be of great help in solving complicated inverse problems. In the case of the tomography of the dielectric tensor field usually no such information is available. At the same time in stress field tomography one may use the equations of the theory of elasticity as *a priori* information. That explains why today we have no practical algorithms for the tomography of the dielectric tensor field, except for some particular cases, but have several algorithms for the tomography of the stress field.

Let us mention that in the case of plane deformation, the axial stress distribution can be determined with the methods of scalar field tomography, since only the axial stress influences the polarization [9]. This permits measurement of the axial stress distribution in optical fibres and fibre preforms of arbitrary cross-section [27]. The other stress components can be calculated with a method of hybrid mechanics [28,29].

A 3D stress field can be characterized also by scalar functions like the first invariant of the stress tensor:

$$I_1 = \sigma_1 + \sigma_2 + \sigma_3. \tag{5.1}$$

It has been established that the coefficient of the extinction of X-rays depends linearly on I_1. On this basis X-ray tomography has been applied to the measurement of the field of I_1 in certain constructions [30].

5.1. The method of Sharafutdinov

Sharafutdinov [4,31] suggested the following method for the measurement of the normal stress in a section of a test object of arbitrary shape. Let us assume that by photoelastic tomographic measurements the specimen is rotated around the z axis (Fig. 4). Tomographic photoelastic measurements are carried out in two parallel sections, $z = z_0$ and $z = z_0 + \Delta z$. For many light rays the parameter of the isoclinic α and the relative optical retardation Δ_* are measured. Thus, experimentally the algorithm is based on Eqs (2.16) and (2.17), which in this case take the form

$$V_1 = \Delta_* \cos 2\alpha = C \int (\sigma_z - \sigma'_x) \mathrm{d}y', \tag{5.2}$$

$$V_2 = \Delta_* \sin 2\alpha = 2C \int \tau_{x'z} \mathrm{d}y'. \tag{5.3}$$

Besides, the value of σ_z at the boundary has to be measured. This can be done by increasing the number of photoelastic measurements of the average axial stress near the boundary and by extrapolating the results to the boundary. That is a generalization of the method proposed by Cheng [32] for stress measurement at the surface of axisymmetric specimens of arbitrary shape [4,31].

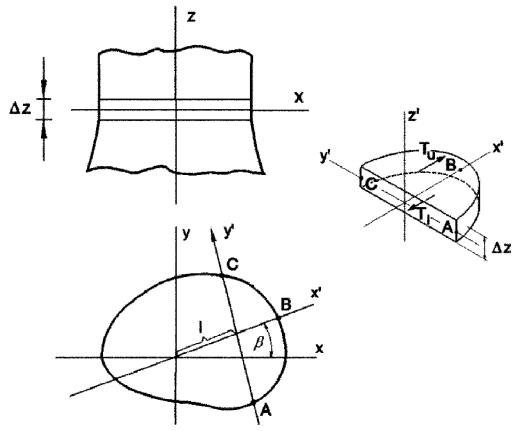

Fig. 4. Explanation of the tomographic measurement schema.

Applying the transverse ray transform [4] to the functions V_1 and V_2 and using equations of equilibrium, determination of the field of σ_z is reduced to a boundary value problem for the Poisson equation. Sharafutdinov has shown that solution of this tomographic problem is unique and only the distribution of σ_z can be determined in this way. However, by rotating the specimen around different axes in tomographic measurements, all the components of the stress tensor can be determined.

A drawback of this method is that the boundary values of σ_z have to be determined with a method of extrapolation. That demands additional measurements near the boundary. Besides, this method is applicable only if the contour of the cross-section is a convex curve.

5.2. The method of decomposition

Since Radon inversion for the tensor field does not exist, the problem of stress field tomography can be solved if we can decompose it to several problems of scalar field tomography for different components of the stress tensor. This can be done in the following way [9,33]. Let us assume that photoelastic tomographic measurements have been carried out in two parallel sections, at a distance of Δz from each other, rotating the specimen around the z axis (Fig. 4).

We denote the values of the functions V_1 and V_2 in the auxiliary section as V_1' and V_2'. Considering the equilibrium of the 3D segment ABC in the direction of the x' axis (Fig. 4), we can write

$$\Delta z \int_A^C \sigma_{x'} \mathrm{d}y' = T_\mathrm{u} - T_\mathrm{l}, \tag{5.4}$$

where T_u and T_l are the shear forces on the upper and lower surfaces of the segment, respectively:

$$T_\mathrm{u} = \frac{1}{2C} \int_l^B V_2' \mathrm{d}x', \quad T_\mathrm{l} = \frac{1}{2C} \int_l^B V_2 \mathrm{d}x'. \tag{5.5}$$

Taking into consideration relationships (5.4) and (5.5), we get from Eq. (5.2)

$$\int_A^C \sigma_z \mathrm{d}y' = \frac{1}{2C\Delta z} \left(\int_l^B V_2' \mathrm{d}x' - \int_\mathrm{l}^B V_2 \mathrm{d}x' \right) - \frac{V_1}{C}. \tag{5.6}$$

Since tomographic photoelastic measurement data can be obtained for all light rays y' in the xy plane, Eq. (5.6) expresses the Radon transform of the field of the stress σ_z. Thus, we have reduced a problem of tensor field tomography to a problem of scalar field tomography for a single stress component σ_z. The field of σ_z can be determined using any of the well-known Radon inversion techniques [1,2]. By rotating the specimen around the x and y axes, in tomo-

graphic measurements fields of σ_x and σ_y can also be determined. Tomographic measurements by rotating the specimen around additional three axes give all the components of the stress tensor.

This method has been implemented with an automatic polariscope AP-04 SM (Fig. 5) [33]. The algorithm of tomographic photoelasticity assumes that optical retardation and the parameter of the isoclinic are measured experimentally. Besides, the direction of the first principal stress σ_1 has to be determined. For that purpose a specific phase-stepping algorihm [34] is used. The polariscope AP-04 SM is controlled by an IBM Thinkpad.

For automatic rotation of small specimens a rotary stage has been constructed. Rotation is effectuated with a stepper motor which permits rotation of the specimen with a precision of 0.1 deg. The specimen is fixed to the rotary stage so that the investigated part of it is placed in an immersion tank.

We illustrate the method with two examples.

First, stresses in a high-pressure lamp (Fig. 6a) were measured. The lamp has mostly axisymmetric form and stresses can be measured with axisymmetric algorithms of integrated photoelasticity [9]. In section AB of the stem, which is not axisymmetric, the normal stress field was determined with photoelastic tomography (Fig. 6b).

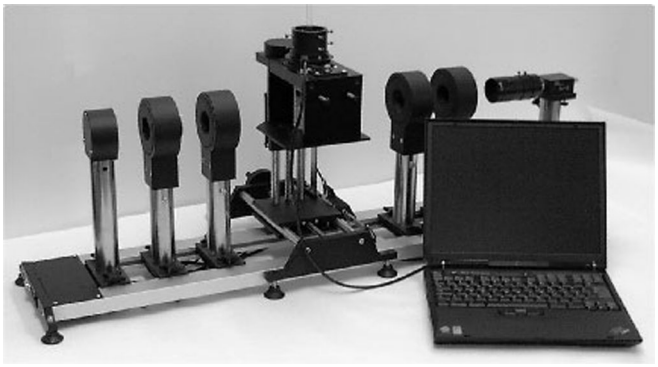

Fig. 5. Computer-controlled polariscope AP-04 SM. The coordinate device with a rotary stage for small test objects is in the middle of the picture.

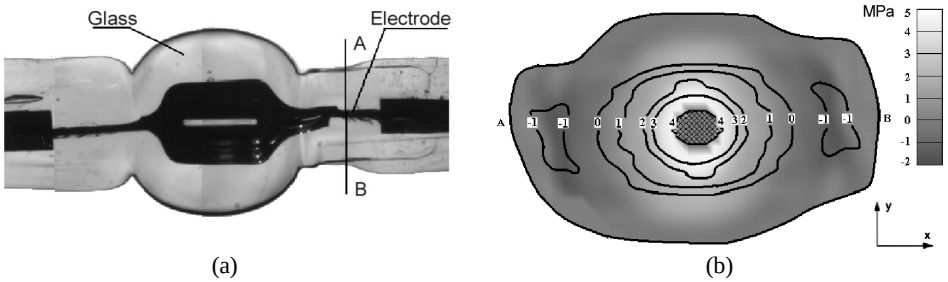

(a) (b)

Fig. 6. Geometry of the high-pressure lamp (a) and normal stress field in section AB (b).

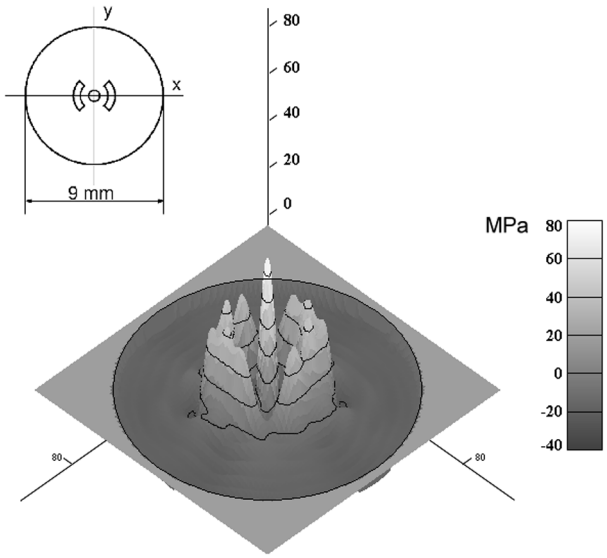

Fig. 7. Cross-section of a bow-tie optical fibre preform and distribution of the axial stress.

In tomographic measurements 180 projections were used. The stress field was calculated with the algorithm of Cormack [35]. Since residual stress should be in equilibrium, the value of the average stress permits estimation of the precision of measurements. In this case the average stress was 0.2 MPa, making about 4% of the maximum value of the stress.

Figure 7 shows the geometry of a cross-section of a bow-tie fibre preform and the axial stress field. In tomographic photoelastic measurements 180 projections were used. For each projection about 100 measurements per millimetre were made. The average value of the axial stress was –2.9 MPa, that is, less than 5% of the maximum tensile stress in the stress-inducing parts. Thus the precision of the measurements is satisfactory.

CONCLUSIONS

We have shown that in formulating the problem of optical tensor field tomography the technology of optical measurements has to be taken into account. The tomographic algorihm in the case of interferometric measurements is completely different from that in the case where only relative optical reatardations are measured. Ignoring this may lead to imaginary tomographic algorithms. It is outlined that an important difference between the tomographic algorithms of the dielectric tensor and stress tensor fields is that in the second case *a priori* information is available in the form of equations of the theory of elasticity. This has helped to develop two algorithms of stress field tomography. Application of one algorithm is demonstrated with two practical examples.

ACKNOWLEDGEMENT

The support of the Estonian Science Foundation (grant No. 6881) is gratefully acknowledged.

REFERENCES

1. Herman, C. T. *Image Reconstruction from Projections*. Academic Press, New York, 1980.
2. Kak, C. A. and Slaney, M. *Principles of Computerized Tomography*. IEEE Press, New York, 1988.
3. Aben, H., Idnurm, S. and Puro, A. Integrated photoelasticity in case of weak birefringence. In *Proceedings of 9th International Conference on Experimental Mechanics, Vol. 2*. Copenhagen, 1990, 867–876.
4. Sharafutdinov, V. A. *Integral Geometry of Tensor Fields*. VSP, Utrecht, The Netherlands, 1994.
5. Pikalov, V. V. and Melnikova, T. S. *Tomography of Plasmas*. Nauka SO, Novosibirsk, 1995 (in Russian).
6. Hertz, H. M. Kerr effect tomography for nonintrusive spatially resolved measurements of asymmetric electric field distributions. *Appl. Opt.*, 1986, **25**, 914–921.
7. Aben, H. K. Kerr effect tomography for general axisymmetric field. *Appl. Opt.*, 1987, **26**, 2921–2924.
8. Kuske, A. and Robertson, G. *Photoelastic Stress Analysis*. J. Wiley, London, 1974.
9. Aben, H. and Guillemet, C. *Photoelasticity of Glass*. Springer, Berlin, 1993.
10. Aben, H. Optical phenomena in photoelastic models by the rotation of principal axes. *Exp. Mech*., 1966, **6**, 13–22.
11. Aben, H. *Integrated Photoelasticity.* McGraw-Hill, New York, 1979.
12. Aben, H. Characteristic directions in optics of twisted birefringent media. *J. Opt. Soc. Am. A*, 1986, **3**, 1414–1421.
13. Mangal, S. K. and Ramesh, K. Determination of characteristic parameters in integrated photoelasticity by phase-shifting technique. *Opt. Lasers Eng*., 1999, **31**, 263–278.
14. Tomlinson, R. A. and Patterson, E. A. The use of phase-stepping for the measurement of characteristic parameters in integrated photoelasticity. *Exp. Mech*., 2002, **42**, 43–50.
15. Kubo, H. and Nagata, R. Determination of dielectric tensor fields in weakly inhomogeneous anisotropic media. *J. Opt. Soc. Am*., 1979, **69**, 604–610.
16. Andrienko, Y. A. and Dubovikov, M. S. Optical tomography of tensor fields: the general case. *J. Opt. Soc. Am. A*, 1994, **11**, 1628–1631.
17. Berezhna, S. Yu., Berezhnyi, I. V. and Vlokh, O. G. Optical tomography of anisotropic inhomogeneous medium. In *Proceedings of 10th International Conference on Experimental Mechanics, Vol. 1*. Lisbon, 1994. Balkema, Rotterdam, 431–435.
18. Wijerathne, M. L. L., Oguni, K. and Hori, M. Tensor field tomography based on 3D photoelasticity. *Mech. Materials*, 2002, **34**, 533–545.
19. Puro, A. E. On tomographic magnetophotoelasticity. *Optics. Spectrosc*., 1996, **81**, 119–125.
20. Aben, H., Idnurm, S., Josepson, J., Kell, K.-J. and Puro, A. Optical tomography of the stress tensor field. In *Analytical Methods for Optical Tomography* (Levin, G. G., ed.), *Proc. SPIE*, 1991, **1843**, 220–229.
21. Schupp, D. Optische Tensortomographie zur Bestimmung räumlicher Spannungs-verteilungen. *Tech. Mess.*, 1999, **66**, 54–60.
22. Schupp, D. Optische Tensortomographie zur Untersuchung räumlicher Spannungsverteilungen. *Fortschritt – Berichte VDI, Reihe 8*, 2000, 858.
23. Kubo, H. and Nagata, R. Determination of dielectric tensor fields in weakly inhomogeneous anisotropic media. II. *J. Opt. Soc. Am*., 1981, **71**, 327–333.

24. Kubo, H. Approach to dielectric tensor slice-type tomography. *J. Opt. Soc. Am. A*, 1997, **14**, 2299–2313.
25. Aben, H. K. and Josepson, J. On the investigation of axisymmetric dielectric tensor fields by integrated photoelasticity. In *Photoelasticity in Engineering Practice* (Paipetis, S. A. and Holister, G. S., eds). Elsevier Applied Science Publishers, London, 1985, 103–132.
26. Hammer, H. and Lionheart, R. B. Reconstruction of spatially inhomogeneous dielectric tensors through optical tomography. *J. Opt. Soc. Am. A*, 2005, **22**, 250–255.
27. Abe, T., Mitsunaga, Y. and Koga, H. Photoelastic computer tomography: a novel measurement method for axial residual stress profile in optical fibers. *J. Opt. Soc. Am. A*, 1986, **3**, 133–138.
28. Puro, A. E. and Kell, K.-J. E. Complete determination of stress in fiber preforms of arbitrary cross-section. *J. Lightwave Technol.*, 1992, **10**, 1010–1014.
29. Park, Y., Paek, U. and Kim, D. Y. Complete determination of the stress tensor of a polarization-maintaining fiber by photoelastic tomography. *Opt. Lett.*, 2002, **27**, 1217–1219.
30. Gorazdovskij, T. Yu., Vainberg, E. I. and Faingoiz, M. L. Investigation of 3D stress-strain fields with X-ray computer tomography. In *Proceedings of 2nd All-Union Symposium on Computerized Tomography*. Kujbyshev, 1985, 46 (in Russian).
31. Sharafutdinov, V. On integrated photoelasticity in case of weak birefringence. *Proc. Estonian Acad. Sci. Phys. Math*., 1989, **38**, 379–389 (in Russian).
32. Cheng, Y. F. Stress at notch root of shafts under axially symmetric loading. *Exp. Mech*., 1970, **10**, 534–576.
33. Aben, H., Errapart, A., Ainola, L. and Anton, J. Photoelastic tomography for residual stress measurement in glass. *Opt. Eng*., 2005, **44**, 093601.
34. Aben, H., Ainola, L. and Anton, J. Half-fringe phase-stepping with separation of the principal stress directions. *Proc. Estonian Acad. Sci. Eng*., 1999, **5**, 198–211.
35. Cormack, A. M. Representation of a function by its line integrals, with radiological applications. *J. Appl. Phys*., 1963, **34**, 2722–2727.

Tensorvälja optilise tomograafia reaalsetest ja irreaalsetest algoritmidest

Hillar Aben, Andrei Errapart ja Leo Ainola

On näidatud, et optilise tensorvälja tomograafia algoritmide koostamisel on vajalik arvestada optiliste mõõtmiste metoodikat. Absoluutsete optiliste käiguvahede interferomeetrilisel mõõtmisel erinevad polariseeritud valguse levikut kirjeldavad võrrandid põhimõtteliselt juhust, mil mõõdetakse vaid relatiivseid optilisi käiguvahesid. Selle erinevuse ignoreerimine võib viia ebareaalsete algoritmideni. Oluliseks erinevuseks dielektrilise tensori välja ja pingetensori välja tomograafilisel määramisel on asjaolu, et teisel juhul saab aprioorse informatsioonina kasutada elastsusteooria võrrandeid. See on võimaldanud pingetensori välja määramiseks välja töötada kaks tomograafilist algoritmi, millest ühe praktilist kasutamist on illustreeritud rakendusnäidetega.